Input-Admittance Calculation and Shaping for Controlled Voltage-Source Converters

Lennart Harnefors, *Senior Member, IEEE*, Massimo Bongiorno, *Student Member, IEEE*, and Stefan Lundberg, *Member, IEEE*

***Abstract*—A controlled power electronic converter can cause local instabilities when interacting with other dynamic subsystems in a power system. Oscillations at a certain frequency cannot, however, build up if the converter differential input admittance has a positive conductance (real part) at that frequency, since power is then dissipated. In this paper, input-admittance expressions for a voltage-source converter are derived. It is seen how the admittance can be shaped in order to get a positive real part in the desired frequency regions by adjusting the controller parameters.**

***Index Terms*—Converter control, dissipativeness, grid interaction, oscillations, passivity, stability.**

I. Introduction

CONTROLLED power electronic converters are increasingly being used in power systems, e.g., distributed generation, high-voltage dc (HVDC) transmissions, flexible ac transmission system devices, and back-to-back inverter drives. While some of these offer better controllability and improvement of global power-system stability, there is also an increased risk for local instabilities, which start as parasitic small-signal oscillations. Among such, we find the subsynchronous torsional oscillations potentially caused by HVDC terminals [1], [2], instabilities in dc power systems [3], dc-link instabilities of inverter drives [4], and oscillations due to converter interactions in single-phase rail networks [5]–[7] as well as in three-phase networks [8], [9].

One cause for instability is constant-power control [4]. Suppose that in a dc system the input power $P = vi$ to a converter is controlled to a constant value. For perturbations Δi about the mean current i_0 and similarly for the voltage, we have

$$v = v_0 + \Delta v = \frac{P}{i_0 + \Delta i} \approx \frac{P}{i_0}\left(1 - \frac{\Delta i}{i_0}\right) \qquad (1)$$

so the converter acts as a differential negative resistance $-P/i_0^2$ for a positive input power. Another cause for instability is, in some cases, the dynamics of the ac control loop together with the pulsewidth modulator (PWM) in a voltage-source converter (VSC) [2], [10].

Manuscript received November 8, 2006; revised June 18, 2007. This work was supported in part by High Voltage Valley.

L. Harnefors is with ABB Power Systems, 771 80 Ludvika, Sweden, and also with Chalmers University of Technology, 412 96 Göteborg, Sweden (e-mail: lennart.harnefors@se.abb.com).

M. Bongiorno and S. Lundberg are with Chalmers University of Technology, 412 96 Göteborg, Sweden (e-mail: massimo.bongiorno@chalmers.se; stefan.lundberg@chalmers.se).

Digital Object Identifier 10.1109/TIE.2007.904022

Whatever the cause of instability, it is clear that if the converter acts as a passive system [11], [12], i.e., the differential input admittance (henceforth called just the input admittance, for simplicity) has nonnegative conductance (i.e., nonnegative real part) for all frequencies, then it cannot generate instabilities. While this is rarely the case, instabilities tend not to occur if the conductance is positive in a neighborhood of each critical resonance, which was shown for torsional resonances in [10].

However, a very simple converter model was considered in [10]: the current control loop only. The contributions of this paper are closed-loop stability analysis of the converter–grid interaction using impedance and admittance matrices; expressions for the elements of the VSC input-admittance matrix, in which also the direct-voltage and alternating-voltage control loops, the phase-locked loop (PLL) used for synchronization, and the dead time (computational and switching time delay) are modeled; controller design recommendations; and verification of the theory using a grid model as well as experiments.

While converter–grid interaction and stability (for VSCs as well as diode and thyristor converters) have been considered in several papers, particularly those cited above, this paper is believed to be the first to tackle the problem using the converter input admittance for three-phase systems. (References [5] and [7] consider input admittances or impedances for single-phase systems.) The main benefit of the method lies in its generality: any grid impedance—symmetric or unsymmetric—can be modeled, while a modification of the VSC control system simply implies finding another input-admittance matrix.

This paper is organized as follows: In Section II, the system model is reviewed. In Section III, the control system is designed and analyzed, where we obtain expressions for the elements of the input-admittance matrix. In Section IV, this matrix is analyzed numerically and analytically. It is seen how the input admittance can be shaped by suitably selecting the controller parameters. This allows the negative conductance region to be reduced as specified (although sometimes at the expense of dynamic performance). Finally, in Section V, the closed-loop system formed through interconnection with the grid is studied, and the results are verified experimentally.

II. System Model

As shown in [13], complex space vectors—denoted with boldface letters—e.g., $\mathbf{v} = v_d + jv_q$ and $\mathbf{i} = i_d + ji_q$ for voltage and current, respectively, and complex transfer functions, e.g., the input admittance $\mathbf{Y}(s) = Y_d(s) + jY_q(s)$, giving

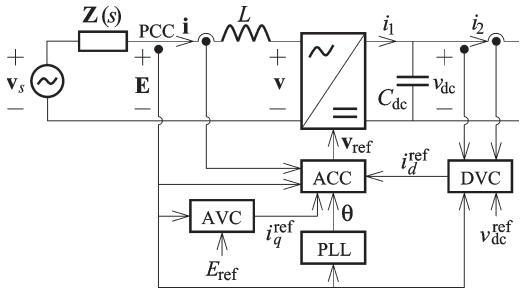

Fig. 1. VSC main circuit diagram and control system.

$\mathbf{i} = \mathbf{Y}(s)\mathbf{v}$,[1] are convenient for the modeling of symmetric three-phase systems, which have balanced phase impedances. However, for unsymmetric systems, it is necessary to use the corresponding real space vectors—denoted with italic letters—e.g., $v = [v_d, v_q]^T \leftrightarrow \mathbf{v}$ and $i = [i_d, i_q]^T \leftrightarrow \mathbf{i}$. Their relation is described by an *input-admittance matrix*

$$i = Y(s)v, \qquad Y(s) = \begin{bmatrix} Y_{dd}(s) & Y_{qd}(s) \\ Y_{dq}(s) & Y_{qq}(s) \end{bmatrix} \tag{2}$$

where, unlike in [13], a positive sign of element (1, 2) is chosen for convenience. [For a symmetric system, $Y_{dd}(s) = Y_{qq}(s) = Y_d(s)$, and $Y_{dq}(s) = -Y_{qd}(s) = Y_q(s)$.] We shall use complex notation to the extent possible, and apply real vectors and transfer matrices only when necessary.

A. Configuration

Consider Fig. 1. The quantities on the three-phase side are expressed in *grid dq frame*, which is defined by the angle θ_1, where $d\theta_1/dt = \omega_1$ is the angular synchronous frequency. $\mathbf{E}$, $\mathbf{i}$, $\mathbf{v}$, and $\mathbf{v}_s$ are the space vectors for the point-of-common-coupling (PCC) voltage, the converter input current, the converter voltage, and the source voltage, respectively. The latter, together with the impedance $\mathbf{Z}(s)$, serves as the grid model. A purely inductive converter input filter with inductance L is assumed. On the dc side, $C_{\rm dc}$ is the dc capacitance, $v_{\rm dc}$ is the direct voltage, while i_1 and i_2 are the input and output (load) currents, respectively.

The ac controller (ACC) has three inputs in addition to the measured quantities $\mathbf{E}$ and $\mathbf{i}$, i.e., the outputs $i_d^{\rm ref}$ and $i_q^{\rm ref}$ of the direct-voltage controller (DVC) and the alternating-voltage controller (AVC), respectively, as well as the transformation angle θ from the PLL. This angle defines the *converter dq frame*, which in the steady state coincides with the grid dq frame. Vectors in the converter dq frame will be denoted with the superscript c. The output is the reference $\mathbf{v}_{\rm ref}$ to the PWM.

The transformations from the grid and converter dq frames to the stationary $\alpha\beta$ frame, e.g., for the PCC voltage, are given by $\mathbf{E}^s = e^{j\theta_1}\mathbf{E}$, and $\mathbf{E}^s = e^{j\theta}\mathbf{E}^c$, respectively. Eliminating $\mathbf{E}^s$ yields the following relation between vectors in the grid and converter dq frames:

$$\mathbf{E}^c = e^{-j\Delta\theta}\mathbf{E}, \quad \Delta\theta = \theta - \theta_1. \tag{3}$$

The error angle $\Delta\theta$ is zero in the steady state but must be taken into account in order to include the PLL dynamics in the system model.

B. Converter–Grid Interconnection and Stability Analysis

If the outer loops (PLL, DVC, and AVC) are disregarded, a symmetric model is obtained (as shown in Section III) as

$$\mathbf{i} = \mathbf{G}_{ci}(s)\mathbf{i}_{\rm ref} + \mathbf{Y}_i(s)\mathbf{E} \tag{4}$$

where $\mathbf{i}_{\rm ref} = i_d^{\rm ref} + ji_q^{\rm ref}$ is the ac reference vector, while $\mathbf{G}_{ci}(s)$ and $\mathbf{Y}_i(s)$ are the ideal (in the sense that the outer loops are disregarded) closed-loop transfer function and input admittance, respectively. $\mathbf{E}$ can be eliminated by using the relation $\mathbf{E} = \mathbf{v}_s - \mathbf{Z}(s)\mathbf{i}$ for the grid model, giving

$$\mathbf{i} = \frac{1}{1 + \mathbf{Y}_i(s)\mathbf{Z}(s)}\left[\mathbf{G}_{ci}(s)\mathbf{i}_{\rm ref} + \mathbf{Y}_i(s)\mathbf{v}_s\right] \tag{5}$$

where $\mathbf{G}_c(s) = \mathbf{G}_{ci}(s)/[1 + \mathbf{Y}_i(s)\mathbf{Z}(s)]$ is the full closed-loop system. For very strong grids, $\mathbf{Z}(s) \approx 0 \Rightarrow \mathbf{G}_c(s) \approx \mathbf{G}_{ci}(s)$.

If the outer loops are taken into account, the system becomes nonlinear but can be linearized by considering perturbation quantities. An unsymmetric model results, so real vectors and transfer matrices must be used, while the matrix inverse replaces division by

$$\Delta i = [I + Y(s)Z(s)]^{-1}\, Y(s)\Delta v_s \tag{6}$$

where $Y(s)$ is the full VSC input-admittance matrix (see the next section), and $Z(s) \leftrightarrow \mathbf{Z}(s)$. Stability can be analyzed by either calculating the poles of the closed-loop system $[I + Y(s)Z(s)]^{-1}$ or applying the multivariable Nyquist criterion to the open-loop transfer matrix $Y(s)Z(s)$ [13].

However, a system cannot cause buildup of oscillation at a certain frequency if it dissipates active power at that frequency. Consequently, stability can generally be guaranteed by making sure that the VSC dissipates power at critical frequencies, particularly poorly damped resonances [10]. Therefore, most of the remainder of this paper is devoted to deriving and studying the input-admittance matrix.

III. Control System Design and Analysis

A. Controller Design Principle

In all control loops except that for the alternating voltage, the controlled process will be found to have integrator characteristics: $G(s) = k/s$. A disturbance d adds at the process input. The disturbance is assumed measurable and can be canceled by feedforward, as shown in Fig. 2.

[1]The Laplace variable s shall be interpreted as the derivative operator $s = d/dt$, where appropriate.

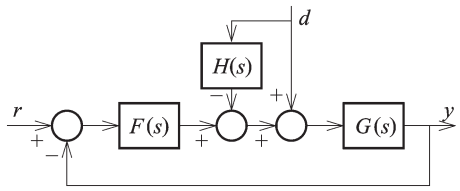

Fig. 2. Closed-loop system with process $G(s)$, controller $F(s)$, and feedforward filter $H(s)$.

With a proportional-plus-integral (PI) controller $F(s) = k_p + k_i/s$ and a first-order low-pass feedforward filter $H(s) = \alpha_f/(s+\alpha_f)$, the transfer functions from reference r to output y (the closed-loop transfer function) and from d to y are

$$G_c(s) = \frac{k(k_p s + k_i)}{s^2 + kk_p s + kk_i}$$
$$G_{dy}(s) = \frac{ks^2}{(s^2 + kk_p s + kk_i)(s+\alpha_f)}. \tag{7}$$

Because of the integrator process characteristics and perfect steady-state feedforward [i.e., $H(0) = 1$], zero steady-state control error and perfect steady-state load-disturbance rejection [i.e., $G_c(0) = 1$ and $G_{dy}(0) = 0$] are obtained even with pure P control ($k_i = 0$). The integral part—if used—may be given just a trimming function that removes steady-state errors resulting from imperfections. Such will be exemplified in the following. This allows selecting a small k_i while letting $k_p = \alpha/k$ to give the bandwidth α in the closed-loop system.

B. AC Control Loop

The ac dynamics in the grid dq frame is given by

$$L\frac{d\mathbf{i}}{dt} + j\omega_1 L\mathbf{i} = \mathbf{E} - \mathbf{v}. \tag{8}$$

Transformation to the converter dq frame, following (3), yields:

$$L\frac{d\mathbf{i}^c}{dt} + j(\omega_1 + \Delta\omega)L\mathbf{i}^c = \mathbf{E}^c - \mathbf{v}^c \tag{9}$$

where $\Delta\omega = d\Delta\theta/dt$ is normally much smaller than ω_1 and can be neglected.

1) Controller Design: A PI current controller with PCC voltage feedforward and cancellation of the dq cross coupling is considered [14] as

$$\mathbf{v}^c_{\text{ref}} = -\left(k_p + \frac{k_i}{s}\right)(\mathbf{i}_{\text{ref}} - \mathbf{i}^c) - j\omega_1 L\mathbf{i}^c + \frac{\alpha_f}{s+\alpha_f}\mathbf{E}^c. \tag{10}$$

(As $\mathbf{i}_{\text{ref}}$ is always expressed in the converter dq frame, it is not denoted by a superscript.) If the controller computational delay and the PWM switching are modeled as a dead time T_d, then $\mathbf{v}^c = e^{-sT_d}\mathbf{v}^c_{\text{ref}}$. However, in order to allow reasonably simple expressions, the dead time will be neglected, except in Section IV-B. For $T_d = 0$, we obtain [cf. (4)]

$$\mathbf{i}^c = \underbrace{\frac{k_p s + k_i}{Ls^2 + k_p s + k_i}}_{\mathbf{G}_{ci}(s)}\mathbf{i}_{\text{ref}} + \underbrace{\frac{s^2}{(Ls^2 + k_p s + k_i)(s+\alpha_f)}}_{\mathbf{Y}_i(s)}\mathbf{E}^c. \tag{11}$$

$\mathbf{G}_{ci}(s)$ and $\mathbf{Y}_i(s)$ are, respectively, identical to $G_c(s)$ and $G_{dy}(s)$ in (7) with $k = 1/L$. Hence, $k_p = \alpha_c L$, where α_c is the current-control-loop bandwidth, can be selected [10], [15]. A small k_i can be employed, as the primary function of the integral part is to remove the steady-state impact of mismatch between actual and model inductances (leading to imperfect decoupling of the d and q axes) and voltage drop across the filter resistance (which is neglected in the model). The design method in [15] recommends selecting k_i as the product of α_c and the filter resistance, which should give a sufficiently small gain. With $k_p = \alpha_c L$ and $k_i \approx 0$, we obtain in real space-vector form

$$i^c = \underbrace{\begin{bmatrix} g_c(s) & 0 \\ 0 & g_c(s) \end{bmatrix}}_{G_c(s)} i_{\text{ref}} + \underbrace{\begin{bmatrix} y_i(s) & 0 \\ 0 & y_i(s) \end{bmatrix}}_{Y_i(s)} E^c \tag{12}$$

where $g_c(s) = \alpha_c/(s+\alpha_c)$, and $y_i(s) = s/[L(s+\alpha_c)(s+\alpha_f)]$.

2) Parameters: Modern transistor PWM converters often employ switching frequencies of 1 kHz and above [14], which enables current response in the millisecond range. A higher angular switching frequency ω_{sw} allows higher bandwidth of the current control loop. In [15], $\alpha_c \leq 0.2\omega_{\text{sw}}$ was recommended. For $\omega_{\text{sw}}/2\pi = 1$ kHz and a 50-Hz base frequency, this yields $\alpha_c \leq 4$ per unit (p.u.).

The input-filter inductance L should be selected inversely proportional to ω_{sw} to give adequate suppression of switching harmonics. Thus, $\alpha_c L$ tends to be an invariant of ω_{sw}, and typically, $\alpha_c L$ is in the range of 1 p.u. (For $\alpha_c = 4$ p.u., $\alpha_c L = 1$ p.u. yields $L = 0.25$ p.u., which is reasonable [14].)

Let us consider the impact of an alternating-voltage disturbance. The current response to a step disturbance $\Delta\mathbf{E}^c$ in the grid voltage is, for $t \geq 0$, given by

$$\Delta\mathbf{i}^c = \mathcal{L}^{-1}\left\{\mathbf{Y}_i(s)\frac{\Delta\mathbf{E}^c}{s}\right\} = \frac{\Delta\mathbf{E}^c}{(\alpha_c - \alpha_f)L}(e^{-\alpha_f t} - e^{-\alpha_c t}) \tag{13}$$

where $\mathcal{L}^{-1}$ indicates the inverse Laplace transform. Relative step responses are depicted for three values of α_f in Fig. 3. As seen, a large α_f is required to give fast rejection with a small $|\Delta\mathbf{i}^c|_{\max}$. This is important in order to avoid overcurrent tripping should grid disturbances (such as voltage swells and sags) occur when the converter is operating at or near the rated current. We shall return to the selection of α_f in Section IV-D.

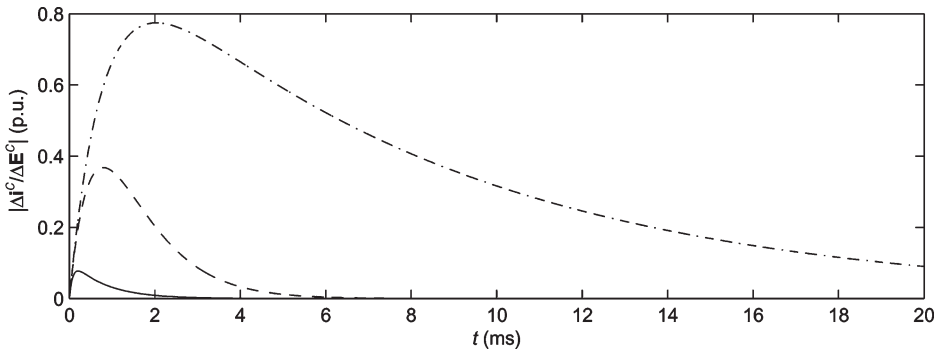

Fig. 3. Disturbance rejection. Relative step responses $|\Delta \mathbf{i}^c/\Delta \mathbf{E}^c|$ for $\alpha_c = 4$ p.u. (solid), $L = 0.25$ p.u. (dashed), and $\alpha_f = \{40, 4, 0.4\}$ p.u. (dashed dotted).

C. Direct-Voltage Control Loop

1) Input Power: To analyze the direct-voltage control loop, linearized expressions for the input power to the VSC are required. The PCC voltage is considered as the phase reference, i.e., $\mathbf{E}$ is real in the steady state. Introducing steady-state and perturbation components as in (1), we get $\mathbf{E} = E_0 + \Delta E_d + j\Delta E_q$, and $\mathbf{i} = i_d^0 + \Delta i_d + j(i_q^0 + \Delta i_q)$. Assuming power-invariant space-vector scaling [13] or p.u. quantities, the instantaneous active and reactive powers flowing into the converter are, respectively, given by

$$P = \mathrm{Re}\{\mathbf{E}\mathbf{i}^*\} \approx \underbrace{E_0 i_d^0}_{P_0} + \underbrace{i_d^0 \Delta E_d + i_q^0 \Delta E_q + E_0 \Delta i_d}_{\Delta P} \tag{14}$$

$$Q = \mathrm{Im}\{\mathbf{E}\mathbf{i}^*\} \approx \underbrace{-E_0 i_q^0}_{Q_0} + \underbrace{i_d^0 \Delta E_q - i_q^0 \Delta E_d - E_0 \Delta i_q}_{\Delta Q}. \tag{15}$$

Opposite to a field-oriented ac drive [14], i_d and i_q are the active- and reactive-power-producing current components, respectively.

2) Controller Design: Assuming a lossless converter and that the ac control loop is much faster than the direct-voltage control loop, the active input power is also the power to the dc link, which gives $i_1 = P/v_{\mathrm{dc}}$. Expressed in the energy $C_{\mathrm{dc}} v_{\mathrm{dc}}^2/2$ stored in the dc capacitor, the dc-link dynamics are given by

$$\frac{1}{2} C_{\mathrm{dc}} \frac{dv_{\mathrm{dc}}^2}{dt} = P - P_L \Rightarrow C_{\mathrm{dc}} v_{\mathrm{dc}}^0 \frac{d\Delta v_{\mathrm{dc}}}{dt} = \Delta P - \Delta P_L \tag{16}$$

where $P_L = v_{\mathrm{dc}} i_2$ is the load power.

If the DVC were to operate directly on the error $v_{\mathrm{dc}}^{\mathrm{ref}} - v_{\mathrm{dc}}$, the closed-loop dynamics would be dependent on the operating point v_{dc}^0. This inconvenience is avoided by selecting the DVC as a PI controller operating instead on the error $[(v_{\mathrm{dc}}^{\mathrm{ref}})^2 - v_{\mathrm{dc}}^2]/2$ [16] with feedforward of the load power (if available for measurement) through a low-pass filter $H_{\mathrm{dc}}(s)$. With the active power reference P_{ref} as the controller output, we get

$$P_{\mathrm{ref}} = \underbrace{\left(k_{pd} + \frac{k_{id}}{s}\right)}_{F_{\mathrm{dc}}(s)} \frac{(v_{\mathrm{dc}}^{\mathrm{ref}})^2 - v_{\mathrm{dc}}^2}{2} + H_{\mathrm{dc}}(s) P_L. \tag{17}$$

In order to reduce the impact of PCC voltage variations on the direct voltage, P_{ref} is then divided by the measured PCC voltage modulus, also filtered through $H_{\mathrm{dc}}(s)$ (to reject high-frequency disturbances) as

$$i_d^{\mathrm{ref}} = \frac{P_{\mathrm{ref}}}{E_f}, \qquad E_f = H_{\mathrm{dc}}(s)|\mathbf{E}|. \tag{18}$$

3) Analysis: Assuming constant $v_{\mathrm{dc}}^{\mathrm{ref}} = v_{\mathrm{dc}}^0$ and $P_L = P_0$, (17) and (18) are linearized as $\Delta P_{\mathrm{ref}} = -v_{\mathrm{dc}}^0 F_{\mathrm{dc}}(s) \Delta v_{\mathrm{dc}}$, giving

$$\begin{aligned} \Delta i_d^{\mathrm{ref}} &= \frac{\Delta P_{\mathrm{ref}}}{E_0} - \frac{P_0}{E_0^2} H_{\mathrm{dc}}(s) \Delta E_d \\ &= -\frac{v_{\mathrm{dc}}^0}{E_0} F_{\mathrm{dc}}(s) \Delta v_{\mathrm{dc}} - \frac{P_0}{E_0^2} H_{\mathrm{dc}}(s) \Delta E_d \end{aligned} \tag{19}$$

and using (12) as

$$\begin{aligned} \Delta i_d = &-\frac{v_{\mathrm{dc}}^0}{E_0} g_c(s) F_{\mathrm{dc}}(s) \Delta v_{\mathrm{dc}} \\ &+ \left[y_i(s) - \frac{P_0}{E_0^2} g_c(s) H_{\mathrm{dc}}(s) \right] \Delta E_d. \end{aligned} \tag{20}$$

Equation (20) is then substituted in (14) and the resulting expression for ΔP in (16). With $i_d^0 = P_0/E_0$, and $i_q^0 = -Q_0/E_0$, we obtain

$$\Delta v_{\mathrm{dc}} = \frac{\left[E_0^2 y_i(s) + P_0 - P_0 g_c(s) H_{\mathrm{dc}}(s)\right] \Delta E_d - Q_0 \Delta E_q}{E_0 v_{\mathrm{dc}}^0 \left[sC_{\mathrm{dc}} + g_c(s) F_{\mathrm{dc}}(s)\right]}. \tag{21}$$

Substitution of (21) back in (19) results in

$$\Delta i_d^{\mathrm{ref}} = -G_{\mathrm{dc}}^d(s) \Delta E_d + G_{\mathrm{dc}}^q(s) \Delta E_q \tag{22}$$

where

$$\begin{aligned} G_{\mathrm{dc}}^d(s) &= \frac{\left[y_i(s) + \frac{P_0}{E_0^2} - \frac{P_0}{E_0^2} g_c(s) H_{\mathrm{dc}}(s)\right] F_{\mathrm{dc}}(s)}{sC_{\mathrm{dc}} + g_c(s) F_{\mathrm{dc}}(s)} + \frac{P_0 H_{\mathrm{dc}}(s)}{E_0^2} \\ G_{\mathrm{dc}}^q(s) &= \frac{Q_0 F_{\mathrm{dc}}(s)}{E_0^2 \left[sC_{\mathrm{dc}} + g_c(s) F_{\mathrm{dc}}(s)\right]}. \end{aligned} \tag{23}$$

4) Parameters: Assuming that the load-power feedforward can be used, the integral part may, also in this case, be given just

a trimming function to compensate for imperfections. As the ac control loop should be much faster than the direct-voltage control loop, the bandwidth α_d of the latter should, as a rule of thumb, be selected as $\alpha_d \leq 0.1\alpha_c$, i.e., a time-scale separation of at least one decade. With a small k_{id}, the characteristic polynomial of (21) is $s + k_{pd}/C_{\rm dc}$ for $g_c(s) \approx 1$, which gives the choice $k_{pd} = \alpha_d C_{\rm dc}$.

It is also reasonable to let the low-pass filter $H_{\rm dc}(s)$ have bandwidth α_d as

$$H_{\rm dc}(s) = \frac{\alpha_d}{s + \alpha_d}. \tag{24}$$

D. Alternating-Voltage Control Loop

This loop is used in static-synchronous-compensator (STATCOM) operation [17]. The idea is to reduce the reactive power at the PCC [i.e., make $i_q < 0$, cf. (15)] when the PCC voltage modulus exceeds its reference $E_{\rm ref}$. A PI AVC is considered as

$$i_q^{\rm ref} = F_{\rm ac}(s)\left(E_{\rm ref} - |\mathbf{E}|\right), \qquad F_{\rm ac}(s) = k_{pa} + \frac{k_{ia}}{s} \tag{25}$$

which is linearized as $\Delta i_q^{\rm ref} = -F_{\rm ac}(s)\Delta E_d$. Together with (22), this can be expressed in real vector form as

$$\Delta i_{\rm ref} = \underbrace{\begin{bmatrix} -G_{\rm dc}^d(s) & G_{\rm dc}^q(s) \\ -F_{\rm ac}(s) & 0 \end{bmatrix}}_{G_{Ei}(s)} \Delta E. \tag{26}$$

As selection of the controller parameters must depend on the grid impedance, no design recommendation for k_{pa} is given, whereas $k_{ia} \approx 0$ is assumed, similar to the other loops.

E. Synchronization Loop (PLL)

1) Design: The PLL acts as a closed control loop—the synchronization loop—which drives the q part of the PCC voltage in the converter dq frame to zero. Assuming that a second-order PLL [18] is used, an instantaneous frequency deviation $\Delta\omega$ is first formed as the output of a PI controller, i.e.,

$$\Delta\omega = \underbrace{\left(k_{pp} + \frac{k_{ip}}{s}\right)}_{F_{\rm PLL}(s)} {\rm Im}\{\mathbf{E}^c\} \tag{27}$$

to which the nominal angular synchronous frequency ω_1^0 (2π times 50 or 60 Hz) is added and integrated into the transformation angle

$$\frac{d\theta}{dt} = \omega_1^0 + \Delta\omega = \omega_1^0 + F_{\rm PLL}(s){\rm Im}\{\mathbf{E}^c\}. \tag{28}$$

From (3), we have

$$\begin{aligned} \mathbf{E}^c &= e^{-j\Delta\theta}\mathbf{E} \approx (1 - j\Delta\theta)(E_0 + \Delta\mathbf{E}) \\ &\approx E_0 + \Delta\mathbf{E} - jE_0\Delta\theta \qquad (29) \\ \Rightarrow {\rm Im}\{\mathbf{E}^c\} &= {\rm Im}\{\Delta\mathbf{E}\} - E_0\Delta\theta \qquad (30) \end{aligned}$$

which gives with $\Delta\theta = \theta - \theta_1$ (where, recall, $d\theta_1/dt = \omega_1$)

$$\frac{d\Delta\theta}{dt} = \omega_1^0 - \omega_1 + F_{\rm PLL}(s)\left({\rm Im}\{\Delta\mathbf{E}\} - E_0\Delta\theta\right). \tag{31}$$

For $\omega_1 = \omega_1^0$, (31) can be put in transfer-function form as

$$\Delta\theta = \underbrace{\frac{F_{\rm PLL}(s)}{s + E_0 F_{\rm PLL}(s)}}_{G_{\rm PLL}(s)} {\rm Im}\{\Delta\mathbf{E}\}. \tag{32}$$

2) Parameters: As ${\rm Im}\{\Delta\mathbf{E}\} = 0$ in the steady state, pure P control, i.e., $F_{\rm PLL}(s) = k_{pp}$, is sufficient to force $\Delta\theta$ to zero when $\omega_1 = \omega_1^0$. The purpose of the integral part is to remove the quasi-steady-state phase error that otherwise would appear when the synchronous frequency deviates from its nominal value. (As ω_1 is not directly measurable, feedforward cannot be used in this case.) Again, the integral gain k_{ip} can be small. By selecting $k_{pp} = \alpha_p/E_0$, the synchronization loop is given the bandwidth α_p as

$$G_{\rm PLL}(s) = \frac{\alpha_p/E_0}{s + \alpha_p} \tag{33}$$

where α_p must be relatively small in order for the PCC voltage harmonics (if present) to be sufficiently rejected [16]. A similar selection as for α_d is suggested: $\alpha_p \leq 0.1\alpha_c$.

3) Analysis: From (29) and (32), it follows that:

$$\Delta\mathbf{E}^c = \Delta\mathbf{E} - jE_0\Delta\theta = \Delta\mathbf{E} - jE_0 G_{\rm PLL}(s){\rm Im}\{\Delta\mathbf{E}\} \tag{34}$$

which in real vector form is given as

$$\Delta E^c = \underbrace{\begin{bmatrix} 1 & 0 \\ 0 & 1 - E_0 G_{\rm PLL}(s) \end{bmatrix}}_{G_{\rm PLL}^s(s)} \Delta E. \tag{35}$$

For the converter input current, the relation $\mathbf{i} = e^{j\Delta\theta}\mathbf{i}^c$ [cf. (3)] is linearized as

$$\Delta\mathbf{i} = \Delta\mathbf{i}^c + j\mathbf{i}_0\Delta\theta = \Delta\mathbf{i}^c + j\mathbf{i}_0 G_{\rm PLL}(s){\rm Im}\{\Delta\mathbf{E}\}. \tag{36}$$

Its real equivalent is, with $i_d^0 = P_0/E_0$ and $i_q^0 = -Q_0/E_0$, given by

$$\Delta i = \Delta i^c + \underbrace{\begin{bmatrix} 0 & (Q_0/E_0)G_{\rm PLL}(s) \\ 0 & (P_0/E_0)G_{\rm PLL}(s) \end{bmatrix}}_{G_{\rm PLL}^p(s)} \Delta E. \tag{37}$$

F. Input Admittance

Equations (12), (26), (35), and (37) form the linearized system depicted in Fig. 4, whose input-admittance matrix is

$$Y(s) = Y_i(s)G_{\rm PLL}^s(s) + G_c(s)G_{Ei}(s) + G_{\rm PLL}^p(s) \tag{38}$$

and whose components are given by

$$\begin{aligned} Y_{dd}(s) &= y_i(s) - g_c(s)G_{\rm dc}^d(s) \\ Y_{qd}(s) &= g_c(s)G_{\rm dc}^q(s) + \frac{Q_0}{E_0}G_{\rm PLL}(s) \\ Y_{dq}(s) &= -g_c(s)F_{\rm ac}(s) \\ Y_{qq}(s) &= y_i(s)\left[1 - E_0 G_{\rm PLL}(s)\right] + \frac{P_0}{E_0}G_{\rm PLL}(s). \end{aligned} \tag{39}$$

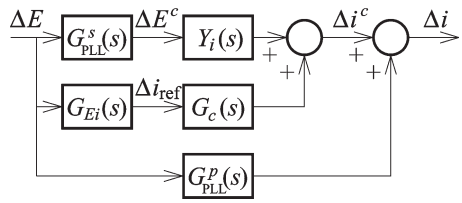

Fig. 4. Block diagram of linearized VSC control system.

For the parameters suggested, these expressions simplify to

$$
\begin{aligned}
Y_{dd}(s) &= \frac{s^2}{L\left(s^2+\alpha_c s+\alpha_c\alpha_d\right)(s+\alpha_f)} \\
&\quad -\frac{P_0}{E_0^2}\frac{\alpha_c\alpha_d(2s+\alpha_d)}{\left(s^2+\alpha_c s+\alpha_c\alpha_d\right)(s+\alpha_d)} \\
Y_{qd}(s) &= \frac{Q_0}{E_0^2}\left[\frac{\alpha_c\alpha_d}{s^2+\alpha_c s+\alpha_c\alpha_d}+\frac{\alpha_p}{s+\alpha_p}\right] \\
Y_{dq}(s) &= -\frac{k_{pa}\alpha_c}{s+\alpha_c} \\
Y_{qq}(s) &= \frac{s^2}{L(s+\alpha_c)(s+\alpha_f)(s+\alpha_p)}+\frac{P_0}{E_0^2}\frac{\alpha_p}{s+\alpha_p}
\end{aligned}
\tag{40}
$$

which will be considered in the next section.

IV. Properties of the Input Admittance

In all numerical evaluations in this section, $L = 0.25$ p.u., $\alpha_c = 4$ p.u., and $E_0 = 1$ p.u. are used.

A. AC Control Loop Only (Ideal Case)

For a symmetric system, it is intuitively clear (and easy to show) that power is dissipated at an angular frequency ω if and only if the input admittance has a positive real part, i.e., $\mathrm{Re}\{\mathbf{Y}(\pm j\omega)\} > 0$ (positive and negative signs to account for positive and negative sequences). A symmetric system is obtained only when the outer loops have negligible dynamics. The negative conductance region of the ideal input admittance $\mathbf{Y}_i(s)$ in (11) is $|\omega| < \omega_{xi}$, where, for $k_p = \alpha_c L$ [10], we have

$$\omega_{xi} = \sqrt{\frac{\alpha_f k_i}{(\alpha_c+\alpha_f)L}}. \tag{41}$$

Since the proposed controller design is based on using a small—or zeroed—integral gain, we note that a nonnegative conductance in the ideal case can be obtained for all frequencies; the system is passive.

B. Impact of Dead Time

If T_d is taken into account, the expression for the ideal input admittance of (11) is generalized to

$$\mathbf{Y}_i(s) = \frac{s+\alpha_f(1-e^{-sT_d})}{L\left[s+\alpha_c e^{-sT_d}+j\omega_1(1-e^{-sT_d})\right](s+\alpha_f)}. \tag{42}$$

The dead time should normally only be a fraction $q < 1$ of the switching period, i.e.,

$$T_d = \frac{2\pi q}{\omega_{\mathrm{sw}}}. \tag{43}$$

Hence, for switching frequencies in the kilohertz range, $T_d <$ 1 ms is reasonable to assume. Suppose that $T_d = 0.5$ ms; with a base frequency of 50 Hz, $T_d = 0.16$ p.u. is obtained. As Fig. 5 shows, this results in a negative conductance frequency region between approximately 9 and 30 p.u. In this region, the inherent damping of passive loads in a power system is normally sufficient to prevent instability [19]. However, problems may possibly arise in smaller isolated grids with several controlled power electronic converters and few passive loads if care is not taken in the design. This has already been acknowledged for single-phase traction grids [6], [7].

An approximate analytic expression for the lower boundary frequency ω_{xt} of the negative conductance region can be derived assuming that $|\omega| \gg \{\omega_1, \alpha_f\}$, which gives

$$\mathbf{Y}_i(j\omega) \approx \frac{1}{L\left(j\omega+\alpha_c e^{-j\omega T_d}\right)}. \tag{44}$$

Solving the positive root of $\mathrm{Re}\{\mathbf{Y}_i(j\omega)\} = 0$ results in

$$\omega_{xt} = \frac{\pi}{2T_d} = \{(43)\} = \frac{\omega_{\mathrm{sw}}}{4q}. \tag{45}$$

For $T_d = 0.16$ p.u., this yields $\omega_{xt} = 10$ p.u., which shows a reasonably good agreement with Fig. 5.

Since the outer loops have impact primarily at lower frequencies, where the impact of the dead time is negligible, we shall henceforth neglect T_d.

C. Power Dissipation of Unsymmetric Systems

To allow assessing the impact of outer loops, a criterion for the power dissipation of unsymmetric systems is needed.

Considering each component of v and i as a complex phasor of angular frequency ω, from standard $j\omega$ calculation, we have $v = Y(j\omega)i$. The active input power is given as $P = \mathrm{Re}\{v_d i_d^* + v_q i_q^*\}$, assuming again power-invariant space-vector scaling or p.u. quantities. This can also be expressed as $P = (1/2)(v^H i + i^H v)$, where the superscript H indicates transpose and complex conjugate (Hermitian conjugate). However

$$v^H i + i^H v = v^H\left[Y(j\omega)+Y^H(j\omega)\right]v \tag{46}$$

where the right-hand side is a quadratic form with the matrix

$$Y(j\omega)+Y^H(j\omega) = \begin{bmatrix} a & c^* \\ c & b \end{bmatrix} \tag{47}$$

whose elements are

$$
\begin{aligned}
a &= Y_{dd}(j\omega)+Y_{dd}^*(j\omega) = 2\mathrm{Re}\left\{Y_{dd}(j\omega)\right\} \\
b &= Y_{qq}(j\omega)+Y_{qq}^*(j\omega) = 2\mathrm{Re}\left\{Y_{qq}(j\omega)\right\} \\
c &= Y_{dq}(j\omega)+Y_{qd}^*(j\omega).
\end{aligned}
\tag{48}
$$

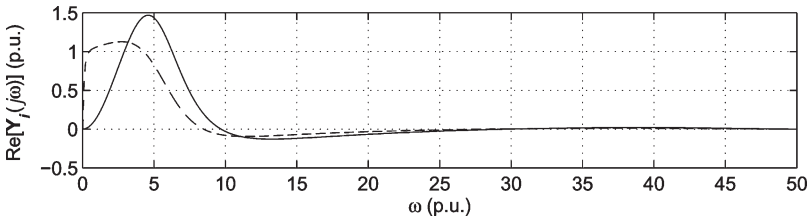

Fig. 5. Impact of dead time. $\mathrm{Re}\{\mathbf{Y}_i(j\omega)\}$ for $T_d = 0.16$ p.u. (solid) and $\alpha_f = \{4, 0.1\}$ p.u. (dashed).

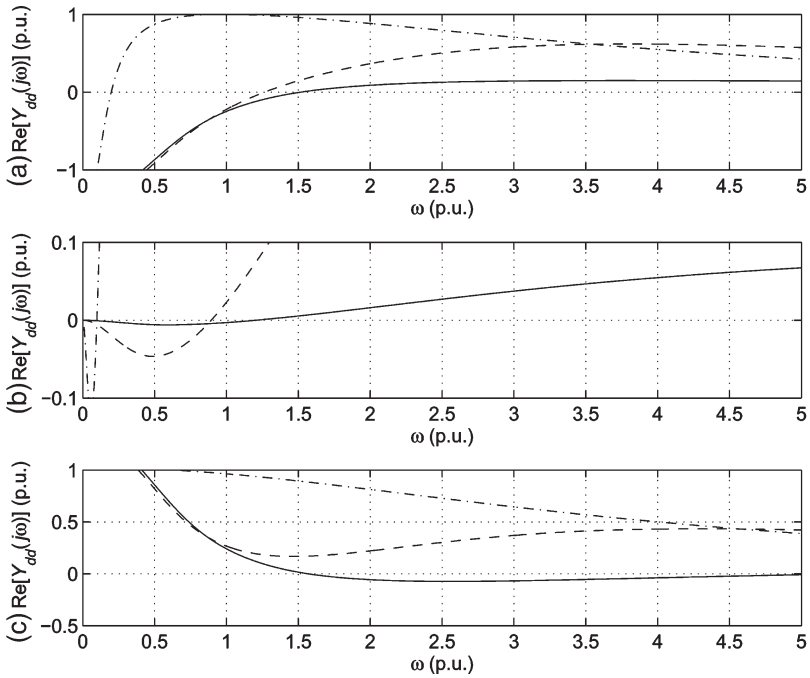

Fig. 6. Impact of the direct-voltage control loop. $\mathrm{Re}\{Y_{dd}(j\omega)\}$ for $\alpha_f = \{40, 4, 0.1\}$ p.u., $\alpha_d = \{0.4, 0.4, 0.1\}$ p.u. (solid, dashed, and dashed dotted, respectively), and (a) $P_0 = 1$ p.u., (b) $P_0 = 0$, and (c) $P_0 = -1$ p.u.

When $Y(j\omega) + Y^H(j\omega) > 0$ (i.e., the matrix is positive definite), (46) is positive, and active power is dissipated [11]. This holds if and only if both eigenvalues $\lambda_{1,2}[Y(j\omega) + Y^H(j\omega)]$ are positive. The characteristic polynomial is given by

$$\det\left[\lambda I - Y(j\omega) - Y^H(j\omega)\right] = (\lambda - a)(\lambda - b) - |c|^2. \quad (49)$$

When $c = 0$, which is obtained for $k_{pa} = Q_0 = 0$, the criterion for power dissipation simplifies to $a > 0$ and $b > 0$, i.e., $\mathrm{Re}\{Y_{dd}(j\omega)\} > 0$ and $\mathrm{Re}\{Y_{qq}(j\omega)\} > 0$. Except for STATCOM operation, this is a realistic assumption, since VSCs are often operated with unity power factor. Therefore, we shall assume $k_{pa} = Q_0 = 0$ except in Section IV-F.

D. Impact of the Direct-Voltage Control Loop

For $Q_0 = 0$, the DVC affects only $Y_{dd}(s)$. Fig. 6 shows curves for rectifier, zero-power, and inverter operation, and three different sets of controller parameters. For inverter operation (i.e., $-1 \le P_0 < 0$ p.u.), it is relatively easy to obtain $\mathrm{Re}\{Y_{dd}(j\omega)\} \ge 0$ for all frequencies.

Poorly damped resonances down to about 10 Hz may exist [19]. Hence, it may in some cases be desired to have $\mathrm{Re}\{Y_{dd}(j\omega)\} > 0$ from frequencies as low as 0.1–0.2 p.u. and up. To achieve this for rectifier operation, both α_f and α_d must be small (never larger than $0.1\alpha_c$, at the very least), which is in conflict with the desire to use a large α_f to avoid overcurrent tripping when rapid changes in the PCC voltage occur (see Section II-B).

One remedy is to use a small α_f during normal mode of operation. If a sudden grid disturbance occurs—which can be detected by monitoring $\mathbf{E}$ and $\mathbf{i}$ and using a suitable criterion—the control system switches to transient mode of operation, where α_f is increased to $\alpha_f \ge \alpha_c$. When a new steady state is attained, α_f is reset to its normal small value. As transient disturbances—e.g., resulting from faults—are normally cleared within a few seconds at most, there is not enough time to build up a subsynchronous oscillation of critically large amplitude, which often takes tens of seconds [19].

A useful expression for the upper boundary frequency ω_{xd} of the negative conductance region can be obtained only for $P_0 = 0$ as

$$\omega_{xd} = \sqrt{\frac{\alpha_c \alpha_d \alpha_f}{\alpha_c + \alpha_f}}. \quad (50)$$

This does not represent a worst-case scenario, but it is seen by comparing Figs. 6(b) and (c) that the ω_{xd}'s for $P_0 = 0$ and $P_0 = 1$ p.u. are at least in the same order of magnitude.

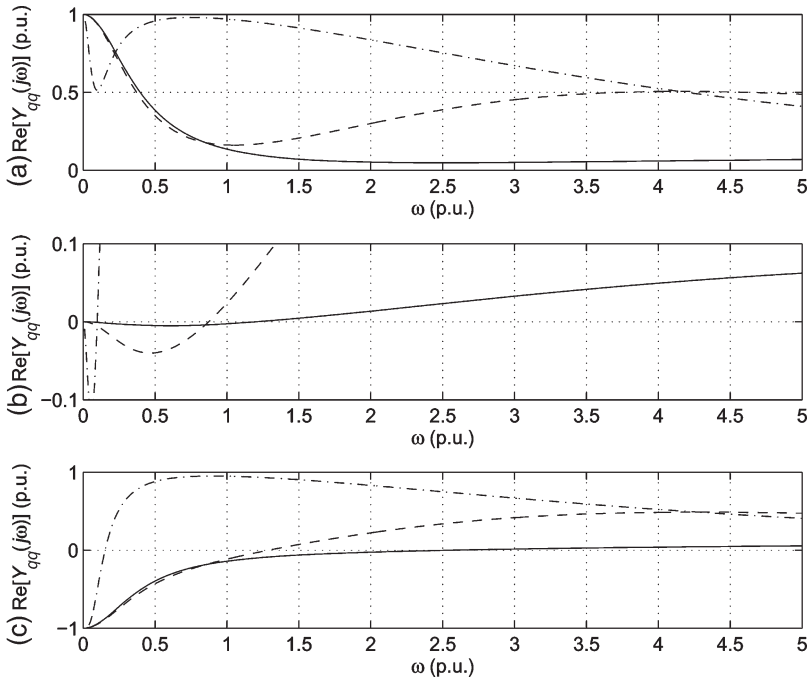

Fig. 7. Impact of the synchronization loop (PLL). $\mathrm{Re}\{Y_{qq}(j\omega)\}$ for $\alpha_f = \{40, 4, 0.1\}$ p.u., $\alpha_p = \{0.4, 0.4, 0.1\}$ p.u. (solid, dashed, and dashed dotted, respectively), and (a) $P_0 = 1$ p.u., (b) $P_0 = 0$, and (c) $P_0 = -1$ p.u.

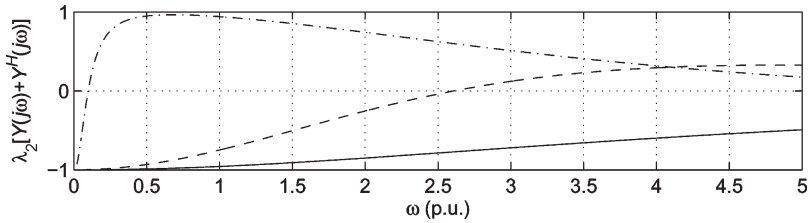

Fig. 8. STATCOM operation with $k_{pa} = 1$ p.u. (solid), $Q_0 = \alpha_d = \alpha_p = 0$ p.u. (dashed), and $\alpha_f = \{40, 4, 0.1\}$ p.u. (dashed dotted).

E. Impact of the Synchronization Loop (PLL)

As Fig. 7 shows, the situation is, in this case, similar to Fig. 6 concerning α_p vis-a-vis α_d, but opposite concerning P_0: the PLL has a negative impact mainly in the inverter mode. Both α_f and α_p must be kept small in order to avoid that $\mathrm{Re}\{Y_{qq}(j\omega)\} < 0$ for most subsynchronous frequencies.

Again, a useful expression for the upper boundary frequency ω_{xp} of the negative conductance region can be obtained only for $P_0 = 0$, i.e.,

$$\omega_{xp} = \sqrt{\frac{\alpha_c \alpha_f \alpha_p}{\alpha_c + \alpha_f + \alpha_p}}. \tag{51}$$

F. Impact of the Alternating-Voltage Control Loop (STATCOM Operation With $P_0 = 0$)

Since $Y(s)$ is not diagonal for STATCOM operation, analysis in this case requires solving the eigenvalues $\lambda_{1,2}$ from (49). A reasonably simple expression can be obtained for the special case of $Q_0 = 0$ and negligible α_d and α_p, i.e.,

$$\lambda_{1,2} = \frac{2(\alpha_c + \alpha_f)\omega^2}{(\omega^2 + \alpha_c^2)\left(\omega^2 + \alpha_f^2\right) L} \pm \frac{k_{pa}\alpha_c}{\sqrt{\omega^2 + \alpha_c^2}}. \tag{52}$$

An expression for the upper boundary frequency ω_{xa} of the negative conductance region (in which $\lambda_2 < 0$) is found by approximating $\omega^2 \ll \alpha_c^2$ as

$$\omega_{xa} = \alpha_c \alpha_f \sqrt{\frac{k_{pa} L}{2(\alpha_c + \alpha_f) - k_{pa}\alpha_c^2 L}}. \tag{53}$$

An approximate agreement with Fig. 8 can be verified. Once again, a small α_f is required to obtain a narrow negative conductance region.

$Q_0 > 0$ and/or nonnegligible (but still reasonably small) α_d and α_p all enlarge the negative conductance region (although not significantly in absolute terms). Letting $Q_0 < 0$ has the opposite effect.

V. Converter–Grid Interconnection and Stability

A. Methodology for Identification of Critical Resonances and Controller Design

Closed-loop current control of a grid-connected VSC has the effect of shifting the locations of the poles (eigenvalues) of the ac network in a similar fashion as closed-loop current control of a field-oriented induction motor (IM) changes the IM's electrical dynamics [14]. The direct-voltage control and

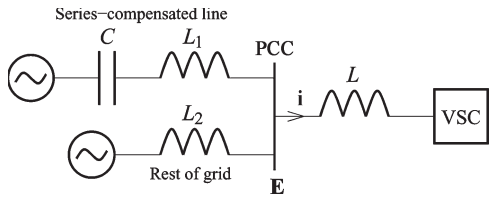

Fig. 9. Network configuration.

synchronization loops are relatively slow, while k_i should be small, so the closed-loop poles obtained for $\{\alpha_d, \alpha_p, k_i\} = 0$ can be assumed to shift just slightly for moderate $\{\alpha_d, \alpha_p, k_i\} > 0$ (with α_c and α_f unchanged, and $k_{pa} = 0$). Hence, the control performance can be evaluated using $\mathbf{G}_c(s) = \mathbf{G}_{ci}(s)/[1 + \mathbf{Y}_i(s)\mathbf{Z}(s)]$, see (5).

However, there is yet a risk that poorly damped resonances may become unstable, i.e., poles with a small real part are moved into the right half of the s plane. This yields the following methodology (which is tested in Section V-B):

1) Find a grid model and determine the grid impedance $\mathbf{Z}(s)$ (note: in synchronous coordinates).
2) Select α_c and α_f; then, find the poles of $1/[1 + \mathbf{Y}_i(s)\mathbf{Z}(s)]$ for $\mathbf{Y}_i(s) = s/[L(s + \alpha_c)(s + \alpha_f)]$. (A symbolic manipulation program such as MAPLE is useful for this task.)
3) Identify critical resonances, i.e., poles with small real part and relatively small imaginary part (low resonant frequency).
4) Select α_d and α_p using the theory of the previous section such that positive conductance of the full input admittance $Y(s)$ is obtained at the critical resonances. (If necessary, modify α_f and repeat from step 2.)

The methodology does not apply to STATCOM operation, since k_{pa} may be large enough to cause significant pole shifting. Studies of this are left to future research.

B. Case-Study Analysis

In the system depicted in Fig. 9, a series-compensated line is connected to the PCC, while the rest of the grid, for simplicity, is modeled as an infinite source in series with an inductance. Including a series resistance r in the resonant circuit, the grid impedance is

$$\mathbf{Z}(s) = \left[r + (s + j\omega_1)L_1 + \frac{1}{(s + j\omega_1)C}\right] \| (s + j\omega_1)L_2. \tag{54}$$

To easily illustrate the phenomena appearing, we in the theoretical analyses consider only the ac control loop, i.e., $\mathbf{Y}_i(s)$ for various k_i. (The impact of the outer loops will be studied experimentally.) In all cases, $L = 0.2$ p.u., and $\alpha_c = \alpha_f = 5$ p.u. Unless noted otherwise, $r = 0$.

1) Full Model: The parameters are $L_1 = L_2 = 0.2$ p.u. and $C = 20$ p.u., i.e., the resonance is, in stationary coordinates, $1/\sqrt{L_1 C} = 0.5$ p.u. This is reasonable; series compensation is normally made such that the resonance becomes subsynchronous [19]. Without control, i.e., $\mathbf{Y}_i(s) = 1/(s + j\omega_1)L$, the poles of $1/[1 + \mathbf{Y}_i(s)\mathbf{Z}(s)]$ are located at $s = \{-j1.4, -j, -j0.59\}$. With control, for $k_i = 0$, we obtain

$$s = \{-3.6 - j2.6, -3.1 + j2.2, -0.00080 - j1.4, -0.00020 - j0.65\}. \tag{55}$$

The pole at $s = -j$ is shifted significantly, but the other two just slightly. (A fourth pole is added due to the dynamics of the PCC voltage feedforward filter.) There are two critical resonances, one of which is subsynchronous. There is a risk for destabilizing this resonance if $\omega_{xi} \geq 0.65$ p.u. Letting $k_i = 0.17$ p.u. yields $\omega_{xi} = 0.65$ p.u.; the poles are then

$$s = \{-3.5 - j2.6, -3.0 + j2.2, -0.00065 - j1.4, 0.0000039 - j0.65, -0.18 - j0.00060\}. \tag{56}$$

Note that the poles, as predicted, shift only slightly when an integral action is included (while a fifth pole is added). The fourth pole is now indeed unstable, but with a very small real part. This indicates that stability should be regained if k_i is decreased, which is easily verified.

For an increase of the integral gain to $k_i = 1$ p.u., $\omega_{xi} = 1.6$ p.u. is obtained. The poles are then

$$s = \{-3.0 - j2.6, -2.4 + j2.3, 0.00026 - j1.4, 0.00038 - j0.65, -1.3 - j0.062\}. \tag{57}$$

Both the third and fourth poles are now unstable, but the real parts are small and tend not to increase as k_i is increased further. This indicates that just a small resistance, in this case $r = 0.0003$ p.u., is sufficient to make the system stable. Hence, series resonances should normally not be troublesome.

2) Very Weak Grid, Parallel Resonance: A large grid inductance in series with a capacitance, e.g., $L_1 = 0$, $L_2 = 1$ p.u., and $C = 0.5$ p.u., is considered, which yields a parallel resonance at $1/\sqrt{L_2 C} = 1.4$ p.u. in stationary coordinates, as seen from the PCC. Without control, the poles are $s = \{-j4.5, j2.5, -j\}$; with control, for $k_i = 0$, they are shifted to

$$s = \{-4.7 - j3.2, -5.1 + j3.0, -0.21 - j2.1, -0.0077 + j0.35\}. \tag{58}$$

There is now a critical resonance at 0.35 p.u. Letting $k_i = 0.049$ p.u. yields $\omega_{xi} = 0.35$ p.u., and the poles

$$s = \{-4.6 - j3.2, -5.1 + j3.0, -0.21 - j2.1, 0.00014 + j0.35, -0.0493 - j0.00098\}. \tag{59}$$

(For a smaller k_i, the system remains stable.) This time, k_i must be kept small even for a fairly large series resistance. For example, it can be verified that $k_i = 0.072$ p.u. is sufficient to give an unstable system with $r = 0.01$ p.u. Hence, instabilities may be hard to prevent for very weak grids with a parallel resonance of fairly low frequency.

3) Series Resonance Connected Radially to VSC: $L_2 = \infty$ in Fig. 9 is now considered, while $L = L_1 = 0.2$ p.u. and $C = 20$ p.u., which give poles at $s = \{-j0.65, -j1.4\}$ without control. Closed-loop ac control has in this configuration the

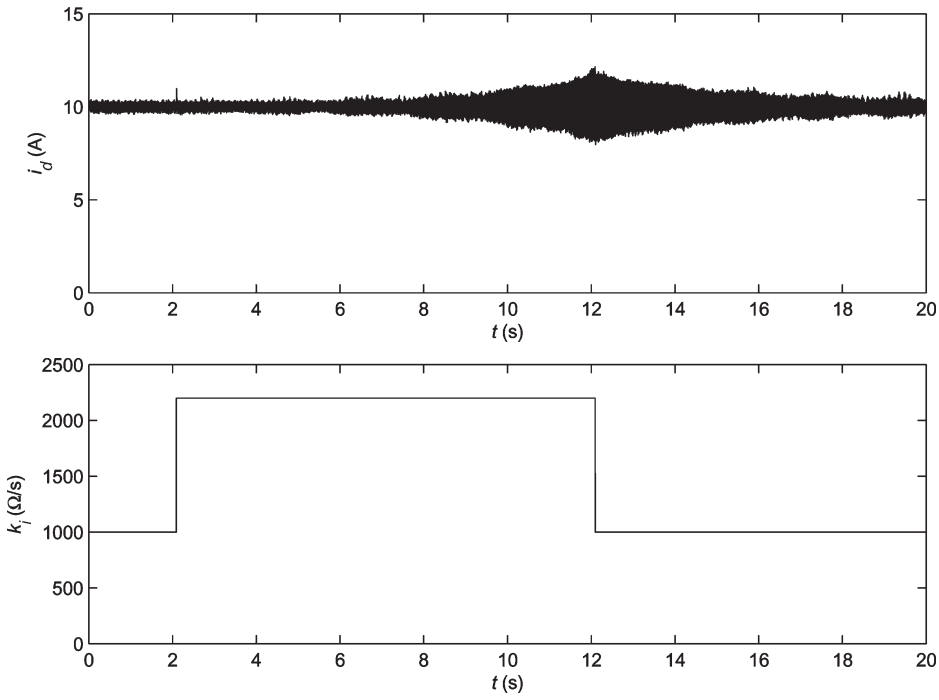

Fig. 10. Impact of the ACC integral part.

somewhat surprising effect of creating a critical resonance at the synchronous frequency. For $k_i = 0$, we have

$$s = \{-2.7 - j2.8, -2.3 + j2.3, -0.0036 - j0.99\}. \quad (60)$$

Consequently, the system should remain stable unless k_i is large enough to make $\omega_{xi} = 1$ p.u. (or higher), which in this case requires $k_i = 0.04$ p.u. The poles are then

$$s = \{-2.5 - j2.8, -2.0 + j2.3, 0.000069 - j0.99, -0.43 - j0.0076\}. \quad (61)$$

Also in this case, a fairly large series resistance, i.e., $r \geq 0.04$ p.u., is required to achieve stability.

Of interest is that the critical resonance remains at the synchronous frequency even when the LC resonance is much higher than 1 p.u. or the circuit reduces to just a capacitance (in series with the VSC filter inductance). Letting $L_1 = 0$ but keeping all other parameters, the following poles are obtained:

$$s = \{-4.7 - j0.47, -4.8 + j0.46, 0.000069 - j0.99, -0.44 + j0.0021\}. \quad (62)$$

C. Experimental Verification

In the experimental setup, a VSC with nominal root mean square phase voltage 69 V (yielding $E_0 = 120$ V for power-invariant space-vector scaling) is used. A radial connection with the circuit parameters $L_1 = 0$, $L_2 = \infty$, $C = 4.0$ mF, $L = 9.0$ mH, $r = 56$ mΩ, and $C_{\rm dc} = 6.6$ mF is studied. The synchronous frequency is 50 Hz, the switching frequency is 5 kHz, and the nominal direct voltage is 350 V, while the ACC parameters are set to $\alpha_c = \alpha_f = 2000$ rad/s.

1) Impact of the ACC Integral Part: From (41), it is found that $\omega_{xi} = 314$ rad/s for $k_i = 1800$ Ω/s. In this experiment, k_i is varied while $\alpha_p = 6.3$ rad/s (yielding negligible impact of the PLL). The direct-voltage control loop is disabled, and a constant direct voltage is supplied from an external source, while $i_d^{\rm ref} = 10$ A is selected. Fig. 10 shows that an instability occurs according to theory. Building up the amplitude of the oscillation takes several seconds.

2) Impact of the DVC: A load resistor of 100 Ω is connected in parallel with the dc capacitor, which results in an active current of $i_d^0 = 10.6$ A and gives $P_0 = 1.3$ kW. The ACC integral gain is zeroed, while $\alpha_p = 6.3$ rad/s is kept. By trial and error, it is found that $\omega_{xd} = 314$ rad/s for $\alpha_d = 45$ rad/s. However, due to the damping of the load resistor and possibly also the series resistance in the ac circuit, the system is stable even for $\alpha_d = 60$ rad/s but turns unstable if α_d is stepped to a higher value, as shown in Fig. 11.

3) Impact of the PLL: The DVC is again disabled, and $i_d^{\rm ref} = -10$ A is used. Equation (51) predicts that $\omega_{xp} = 314$ p.u. for $\alpha_p = 100$ rad/s. As seen in Fig. 12, oscillations commence when α_p is set to 110 rad/s. (Since $k_i = 0$, there is a steady-state current control error.)

VI. Conclusion

In this paper, expressions for the elements of the input-admittance matrix $Y(s)$ of a controlled VSC have been derived. For a certain grid impedance matrix $Z(s)$, the stability of the resulting closed-loop system (6) can be assessed. This can

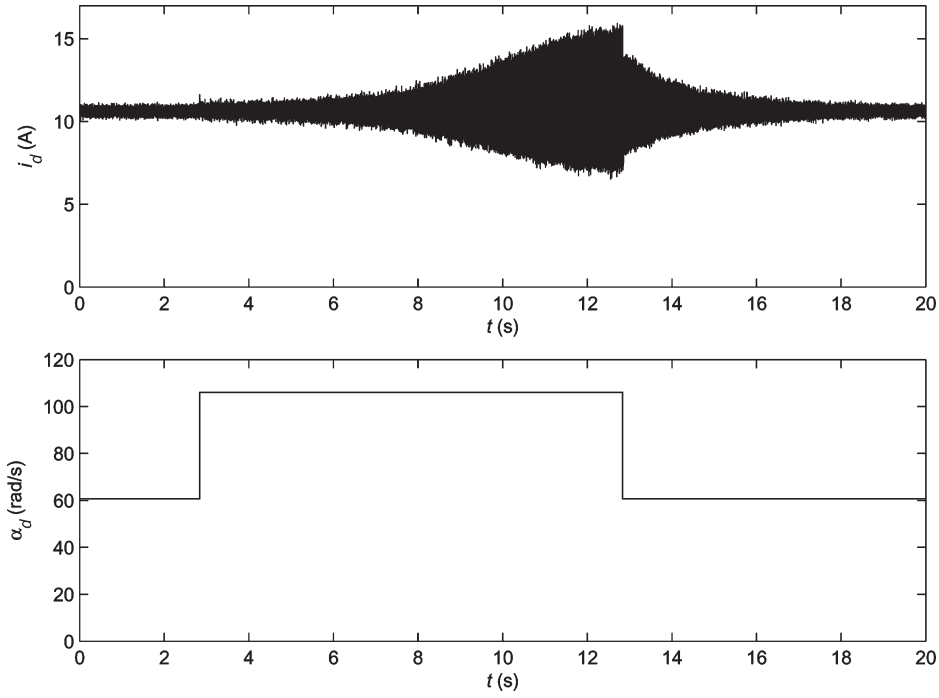

Fig. 11. Impact of the DVC.

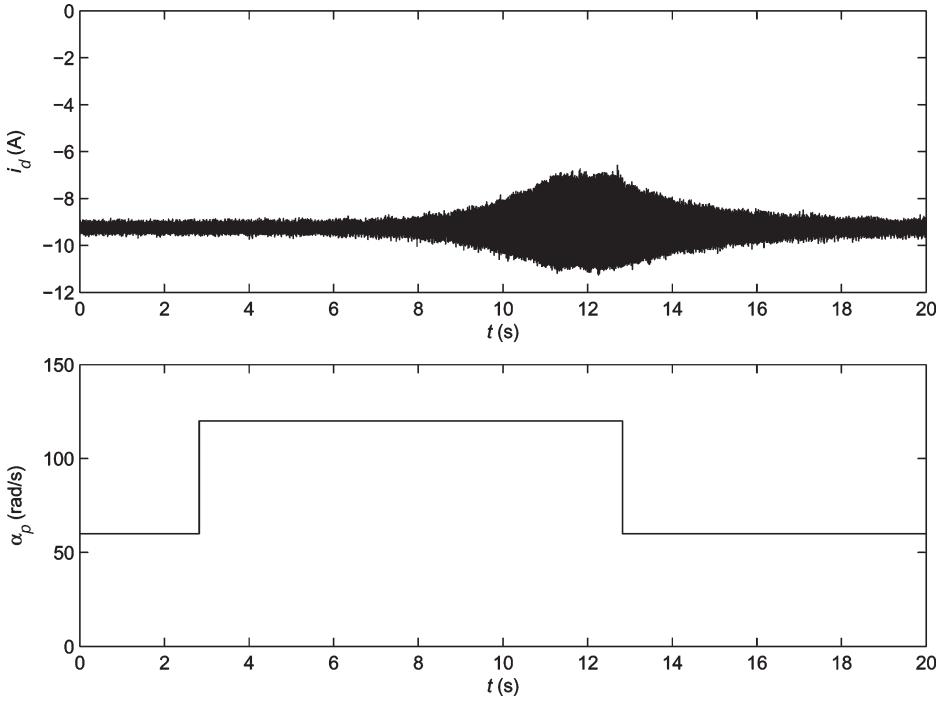

Fig. 12. Impact of the PLL.

be directly applied to VSC controller design, e.g., using the multivariable Nyquist criterion [13].

If $Y(s)$ and $Z(s)$ are both passive, i.e., have positive conductance properties for all frequencies, the closed-loop system is guaranteed to be stable. While a controlled VSC will generally not act as a passive system, it was shown that if $Y(s)$ has positive conductance properties at critical grid resonances, the converter–grid interconnection will generally be stable (one possible exception is monotonic instabilities, i.e., nonoscillative modes with real positive poles [20]).

A step-by-step design methodology based on this finding, including identification of critical (poorly damped, low-frequency) resonances, was presented. The following qualitative controller design recommendations [which are quantified by (41), (50), and (51)] should be observed if there are critical resonances (electrical and/or torsional) present:

- Use a very low integral gain k_i (or no integral part at all) in the ACC. The integral part should have only a trimming function.

- Do not select the bandwidths α_d and α_p of the direct-voltage control and synchronization (PLL) loops larger than necessary; $0.1\alpha_c$ is the upper limit for both.
- Select the bandwidth α_f of the PCC voltage feedforward filter in the ACC fairly low $(\alpha_f \leq 0.1\alpha_c)$ for normal mode of operation but equal to α_c or larger for short-term transient-mode operation.

Scenarios where the theory should find application include—but are not limited to—the following:

- VSC HVDC terminals and other high-power VSCs electrically close to synchronous generators with subsynchronous torsional resonances. Extending the results of Harnefors [10], if $Y(s)$ has positive conductance properties in a neighborhood of each torsional resonance, there should be little risk for destabilization.
- In this paper, very weak grids were modeled as a low parallel LC resonance, which was found to be the most serious case in Section V-B. Extension to more elaborate grid models can be made by considering a different $Z(s)$.
- Isolated grids with several controlled converters and few passive loads, e.g., offshore wind farms with solely full-converter wind-turbine generators. Because a negative conductance region for higher frequencies—cf. (43)—was found to appear when the dead time is nonnegligible, stability problems involving high-frequency oscillations may occur.

Future research may be directed to the further investigation of STATCOM operation, inclusion of more elaborate dc-link models (to account for the source or load to which the dc link is connected), and the possible closed-loop impact of switching harmonics [6].

REFERENCES

[1] M. P. Bahrman, E. V. Larsen, H. S. Patel, and R. J. Piwko, "Experience with HVDC-turbine-generator torsional interaction at Square Butte," *IEEE Trans. Power App. Syst.*, vol. PAS-99, no. 3, pp. 966–975, May 1980.

[2] E. Larsen and I. McIntyre, "Subsynchronous torsional interaction with voltage-source converter HVDC systems—Reference-frame study," GE Power Syst. Energy Consulting, 2001. Final Report.

[3] S. D. Sudhoff, S. F. Glover, P. T. Lamm, D. H. Schmucker, and D. E. Delisle, "Admittance space stability analysis of power electronic systems," *IEEE Trans. Aerosp. Electron. Syst.*, vol. 36, no. 3, pp. 965–973, Jul. 2000.

[4] K. Pietiläinen, L. Harnefors, A. Petersson, and H.-P. Nee, "DC-link stabilization and voltage sag ride-through of inverter drives," *IEEE Trans. Ind. Electron.*, vol. 53, no. 4, pp. 1261–1268, Jun. 2006.

[5] A. Paice and M. Meyer, "Rail network modelling and stability: The input admittance criterion," in *Proc. 14th Int. Symp. Math. Theory Netw. Syst.*, Perpignan, France, Jun. 2000. CD-ROM.

[6] E. Möllerstedt and B. Bernhardsson, "Out of control because of harmonics—An analysis of the harmonic response of an inverter locomotive," *IEEE Control Syst. Mag.*, vol. 20, no. 4, pp. 70–81, Aug. 2000.

[7] M. Jansson, A. Danielsson, J. Galić, K. Pietiläinen, and L. Harnefors, "Stable and passive traction drives," in *Proc. IEEE Nordic Power and Ind. Electron. Conf.*, Trondheim, Norway, 2004. CD-ROM.

[8] A. Emadi, "Modeling of power electronic loads in ac distribution systems using the generalized state-space averaging method," *IEEE Trans. Ind. Electron.*, vol. 51, no. 5, pp. 992–1000, Oct. 2004.

[9] M. Belkhayat, "Stability criteria for ac power systems with regulated loads," Ph.D. dissertation, Purdue Univ., West Lafayette, IN, Dec. 1997.

[10] L. Harnefors, "Analysis of subsynchronous torsional interaction with power electronic converters," *IEEE Trans. Power Syst.*, vol. 22, no. 1, pp. 305–313, Feb. 2007.

[11] J. C. Willems, "Dissipative dynamical systems, Part I: General theory," *Arch. Ration. Mech. Anal.*, vol. 45, no. 5, pp. 321–351, Jan. 1972.

[12] J. C. Willems, "Dissipative dynamical systems, Part II: Linear systems with quadratic supply rates," *Arch. Ration. Mech. Anal.*, vol. 45, no. 5, pp. 352–393, Jan. 1972.

[13] L. Harnefors, "Modeling of three-phase dynamic systems using complex transfer functions and transfer matrices," *IEEE Trans. Ind. Electron.*, vol. 54, no. 4, pp. 2239–2248, Aug. 2007.

[14] B. K. Bose, *Power Electronics and Variable Frequency Drives*. New York: IEEE Press, 1997.

[15] L. Harnefors and H.-P. Nee, "Model-based current control of ac drives using the internal model control method," *IEEE Trans. Ind. Appl.*, vol. 34, no. 1, pp. 133–141, Jan./Feb. 1998.

[16] R. Ottersten, "On control of back-to-back converters and sensorless induction machine drives," Ph.D. dissertation, Dept. Elect. Power Eng., Chalmers Univ. Technol., Göteborg, Sweden, 2003.

[17] A. Jain, K. Joshi, A. Behal, and N. Mohan, "Voltage regulation with STATCOMs: Modeling, control and results," *IEEE Trans. Power Del.*, vol. 21, no. 2, pp. 726–735, Apr. 2006.

[18] G.-C. Hsieh and J. C. Hung, "Phase-locked loop techniques—A survey," *IEEE Trans. Ind. Electron.*, vol. 43, no. 6, pp. 609–615, Dec. 1996.

[19] P. M. Anderson, B. L. Agrawal, and J. E. Van Ness, *Subsynchronous Resonance in Power Systems*. New York: IEEE Press, 1990.

[20] A. Tabesh and R. Iravani, "On the application of the complex torque coefficients method to the analysis of torsional dynamics," *IEEE Trans. Energy Convers.*, vol. 20, no. 2, pp. 268–275, Jun. 2005.

Lennart Harnefors (S'93–M'97–SM'07) was born in Eskilstuna, Sweden, in 1968. He received the M.Sc., Licentiate, and Ph.D. degrees from the Royal Institute of Technology, Stockholm, Sweden, in 1993, 1995, and 1997, respectively, all in electrical engineering, and the Docent (D.Sc.) degree in industrial automation from Lund University, Lund, Sweden, in 2000.

From 1994 to 2005, he was with Mälardalen University, Västerås, Sweden, where he was appointed as a Professor of electrical engineering in 2001. He is currently with ABB Power Systems, Ludvika, Sweden. Since 2001, he has also been a part-time Visiting Professor of electrical drives with Chalmers University of Technology, Göteborg, Sweden. His research interests include applied signal processing and control, in particular, control of power electronic systems and ac drives.

Prof. Harnefors is an Associate Editor of the IEEE TRANSACTIONS ON INDUSTRIAL ELECTRONICS. He was the recipient of the 2000 ABB Gunnar Engström Energy Award and the 2002 IEEE TRANSACTIONS ON INDUSTRIAL ELECTRONICS Best Paper Award.

Massimo Bongiorno (S'02) received the M.Sc. degree in electrical engineering from the University of Palermo, Palermo, Italy, in April 2002 and the Lic.Eng. and Ph.D. degrees from Chalmers University of Technology, Göteborg, Sweden, in December 2004 and September 2007, respectively. He is currently part-time with Chalmers Unversity of Technology and part-time with Gothia Power, Göteborg.

His interests include application of power electronics in power systems and power quality.

Stefan Lundberg (S'04–M'06) was born in Göteborg, Sweden, in 1976. He received the Ph.D. degree in electrical engineering from Chalmers University of Technology, Göteborg, Sweden, in 2007.

He is with the Department of Energy and Environment, Division of Electric Power Engineering, Chalmers University of Technology. His main area of interest is control and modeling of wind parks.